Provided for non-commercial research and education use.
Not for reproduction, distribution or commercial use.

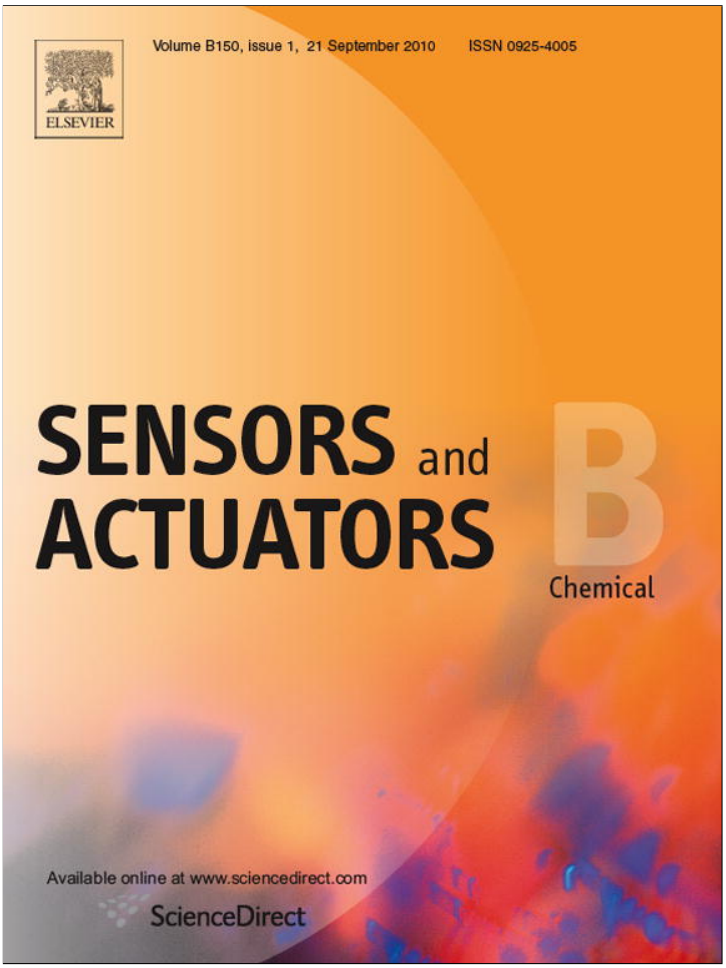

This article appeared in a journal published by Elsevier. The attached copy is furnished to the author for internal non-commercial research and education use, including for instruction at the authors institution and sharing with colleagues.

Other uses, including reproduction and distribution, or selling or licensing copies, or posting to personal, institutional or third party websites are prohibited.

In most cases authors are permitted to post their version of the article (e.g. in Word or Tex form) to their personal website or institutional repository. Authors requiring further information regarding Elsevier's archiving and manuscript policies are encouraged to visit:

http://www.elsevier.com/copyright

Author's personal copy

Sensors and Actuators B 150 (2010) 239–246

Contents lists available at ScienceDirect

Sensors and Actuators B: Chemical

journal homepage: www.elsevier.com/locate/snb

X–Y sample scanning stage and calibration method suitable for single-molecule detection

Ketvalee Treegate[a], Areefen Rasamessard[a], Tanakorn Osotchan[a], Jose Hector Hodak[a,b,*]

[a] Department of Physics, Faculty of Science, Mahidol University, Rama 6 Rd, Phayathai, Bangkok 10400, Thailand
[b] INQUIMAE-Departamento de Química Inorgánica, Analítica y Química Física, Facultad de Ciencias Exactas y Naturales, UBA, Pabellón 2, Ciudad Universitaria, AR-1428 Buenos Aires, Argentina

ARTICLE INFO

Article history:
Received 12 May 2008
Received in revised form 18 June 2010
Accepted 6 July 2010
Available online 14 July 2010

Keywords:
Single molecule spectroscopy
Fluorescence spectroscopy
Optical detection
Scanning confocal microscopy

ABSTRACT

This paper describes the construction of a positioning device for sample scanning in the *x* and *y* directions suitable for single molecule fluorescence experiments. The mechanism uses a simple parallelogram flexure cut out of a single aluminum plate and two amplified piezoelectric actuators of the type used for microscope objective focus adjustment. A displacement range of 75 μm on each axis is obtained. The stage can be used to implement a sample scanning confocal microscope for single molecule spectroscopy applications using either inverted or up-right microscopes. Images with diffraction limited resolution can be obtained with this scanning stage. This is demonstrated by imaging glass beads labeled with the DY475 fluorescent dye and single rhodamine molecules. Micron sized range images of 256 × 256 pixels can be obtained with dwell times down to 0.5 ms/pixel. A novel direct calibration in which the mechanical response obtained from the line profiles for forward and reverse motion is used to account for the hysteresis of the stage. The target molecules are then located within the focus of the laser beam by using its corrected position. The performance of this scanning device and correction technique are demonstrated for the acquisition of fluorescence trajectories of individual rhodamine molecules.

© 2010 Elsevier B.V. All rights reserved.

1. Introduction

In single molecule fluorescence experiments with immobilized molecules it is necessary to scan the sample in *x*–*y* directions in order to locate the target molecules to be studied [1–3]. Normally this is accomplished either by scanning the excitation laser or by moving the sample relative to a stationary laser beam. Sample scanning is advantageous when small area detectors are used. A reproducible and backlash-free mechanical means of scanning the sample in sub-micrometer length scales is necessary to accomplish this goal [1]. There are many commercially available scanning systems that are capable of reproducing motions down to 100 pm. Although the commercial devices have excellent performance characteristics, there is the need for alternative devices with the necessary accuracy and that are simple to build. The design of precision nano-positioning is presently a very active field. Several very innovative topologies capable of subnanometer resolutions were recently reported [4–8]. Experimental systems with diffraction limited spatial resolution do not strictly require a sub-nm position accuracy for successful data collection. In addition, the excitation of fluorescence from single molecules causes irreversible photobleaching after some 10^5–10^6 excitation cycles [9]. The collection efficiency rarely exceeds 20% which translates in 2×10^5 detected photons. This sets an upper bound for the acquisition time of the fluorescence of an individual molecule. For example, if the detected count rate is 5 kHz the average survival time of the molecules will be 40 s. In most cases photobleaching indeed occurs within few tens of seconds. The inherently short lifespan of a molecule under laser excitation greatly relaxes the effects of thermal drift and creep in the scanning stage. Therefore, a realistic minimum specification need only sub-diffraction limit position stability over several tens of seconds. A scanning range of several tens of micrometers would also be a desirable quality. We have constructed a scanning stage based on one of the simplest flexure topologies and used a simple calibration technique to position a laser beam within the diffraction limit accuracy. We evaluated its performance in the acquisition of single molecule fluorescence images and fluorescence trajectories.

2. Instrumentation

The scanning stage is composed of two main components; a guidance mechanism and a pair of piezoelectric actuators. The guidance mechanism is a modified version of the simple-parallelogram flexure mechanism developed by Awtar et al. [4,5] and it is shown

* Corresponding author at: Department of Physics, Faculty of Science, Mahidol University, Rama 6 Rd, Phayathai, Bangkok 10400, Thailand. Tel.: +66 2201 5853.
E-mail addresses: jhodak@qi.fcen.uba.ar, frjhh@mahidol.ac.th (J.H. Hodak).

0925-4005/$ – see front matter © 2010 Elsevier B.V. All rights reserved.
doi:10.1016/j.snb.2010.07.008

Author's personal copy

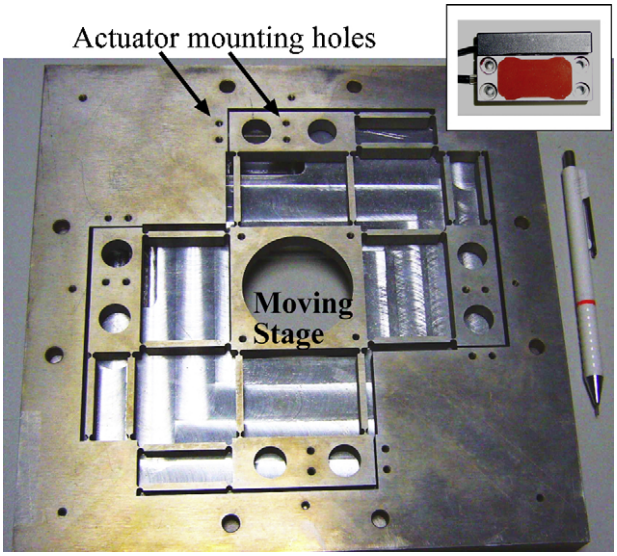

Fig. 1. Photography of the scanning device. The insert shows one of the amplified actuators. The central aperture is approximately 50 mm.

in Fig. 1. This design was chosen because it avoids nesting the displacements in x and y directions. The simple parallelogram flexures used in this work are compliant in one direction but suffer from a parasitic displacement in the direction perpendicular to the travel direction. This parasitic displacement is given by [10]:

$$\Delta e_y = \frac{3\Delta x^2}{5l} \tag{1}$$

For the 39 mm long blades used in our scanning stage and in the event of a scanning displacement of 80 μm, the parasitic displacement is $\Delta e_y \approx 98$ nm. This figure is 50% short of the diffraction limited spot size. Furthermore, typical single molecule experiments demand images spanning areas in the 2 μm × 2 μm to 20 μm × 20 μm range for which the error Δe_y would not impair the image quality.

The parallelogram system presented here uses notch hinges to increase the rigidity of the beams. The entire guidance mechanism was cut out of a 240 mm × 240 mm and 10 mm thick plate of aluminum 5083 alloy using electric discharge machining (EDM) and wire cut techniques. The actuators are mounted on the bottom side of the guidance mechanism with 4 screws.

Piezoelectric stacks are available with displacement ranges in excess of 100 μm. We however, used amplified piezoelectric actuators for powering the scanning stage to achieve a large scanning range. A variety of actuators are commercially available with built in closed loop electronics which minimize the hysteresis and creep, thus improving the position reproducibility [11]. Regular piezoelectric stacks could be used to further reduce the cost of the scanning device, provided that a mechanical amplification mechanism is embedded in the guidance mechanism. Piezoelectric stacks capable of 17 μm are commercially available. A mechanical amplification factor of 6 would provide a scanning range close to 100 μm. The scanning stage design presented here may be easily modified in order to accommodate low cost piezoelectric stacks (cf. supplementary information). Operation in open loop may perform sufficiently well for applications where it is only necessary to collect an image by scanning the sample.

For our construction we used a pair of microscope objective positioners (Piezo Jena MOPOS-100SG) with the objective mounting rings removed from them (Fig. 1 insert). The resulting parallelogram actuators together with the strain gauge are then attached via the four holes that hold the objective mount bound to them. A 6 mm × 16 mm × 0.1 mm rectangular piece of stainless steel shimming stock are used as a spacer between the aluminum guidance plate and the actuators to allow for free parallelogram deformation of the actuators. The aluminum plate together with the actuators is supported on an aluminum block having cavities to house the actuators. The mechanism is protected by a 3 mm thick aluminum plate with an 11 cm × 11 cm central square cutout. A square aluminum plate of 10.9 cm × 10.9 cm × 0.3 cm having a 20 mm circular aperture in the center is mounted on the moving stage. The circular aperture is present to allow a microscope objective to be positioned underneath of the stage, necessary to use the scanning stage in inverted microscopes.

Table 1
Characteristics of the amplified piezoelectric actuators MIPOS-100SG.

Parameter	Open loop	Closed loop
Motion range/μm	100	80
Stiffness/N/μm	1.4	1.4
Reproducibility/nm	30	30
Resonant frequency/Hz	300	300

The piezoelectric actuators used in our stage can produce nominal displacements of 80 μm when driven in the closed loop mode. The actuator specifications that are relevant to this work are shown in Table 1. The position reproducibility of these actuators is 30 nm as specified by the manufacturer. Since the guidance mechanism acts as a lever spring which loads the actuator, we needed to design the dimensions of the parallelogram blades so that the stiffness of the guidance mechanism does not impair the maximum displacement of the unloaded actuators. The geometry and the definition of the parameters for the double notch parallelogram used are shown in Fig. 2. The static stiffness of each parallelogram in the direction of the displacement is given by [10]:

$$K_{\text{par}} = \frac{F_x}{\Delta x} = \frac{16Edt^{5/2}}{9\pi R^{1/2}L^2} \tag{2}$$

where $E = 7.0 \times 10^4$ N/mm^2 is the Young's modulus for the material and d is the depth of the blades. For an actuator with nominal displacement Δx_0 and stiffness K_{act}, the maximum displacement against the parallelogram load is:

$$\Delta x_l = \Delta x_0 \left(\frac{K_{\text{act}}}{K_{\text{act}} + K_{\text{par}}} \right) \tag{3}$$

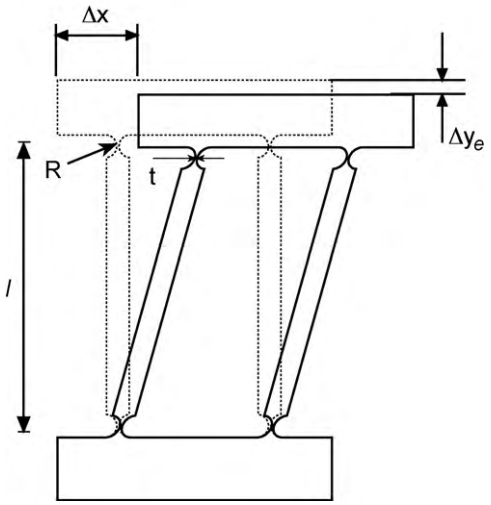

Fig. 2. Schematic showing the definition of the geometric parameters used in the flexure elements of the scanning stage.

Author's personal copy

An important parameter in this design is the minimum thickness of the circular notch hinge due to the strain concentration. The smaller the parameter t, the smaller will be the load on the actuators. Sagging of the stage however may occur for very thin notches. We have chosen 10 mm thick 5083 aluminum alloy plate as the substrate to cut the guidance mechanism. One way to determine the minimum joint thickness emphasizing reliability of the hinge mechanism uses the strain concentration at the joint [10]. Alternatively, overload can lead to irreversible damage of the amplified piezoelectric actuators. The amplified piezoelectric actuators used here were not designed to develop forces larger than 3 N. Thus, we choose to derate the operation of the actuators by limiting the maximum force opposed to them. To determine the minimum thickness of the notches we combined Eqs. (2) and (3) and set the minimum achievable displacement of the stage-actuator assembly to 97% of the nominal motion range of the free actuator. This is equivalent to a derating factor of 1/3 on the absolute maximum force that the actuators are capable of applying. This constrain yielded a minimum thickness of 0.32 mm using 3 mm diameter notches on each end of the 39 mm aluminum blades. The calculated stiffness of each parallelogram mechanism is $K_{par} = 9.80 \times 10^{-3}$ N/μm. Considering the additive effect of 4 double notch parallelograms on each travel direction, the total stiffness of the guiding mechanism is $K_{par} = 3.90 \times 10^{-2}$ N/μm.

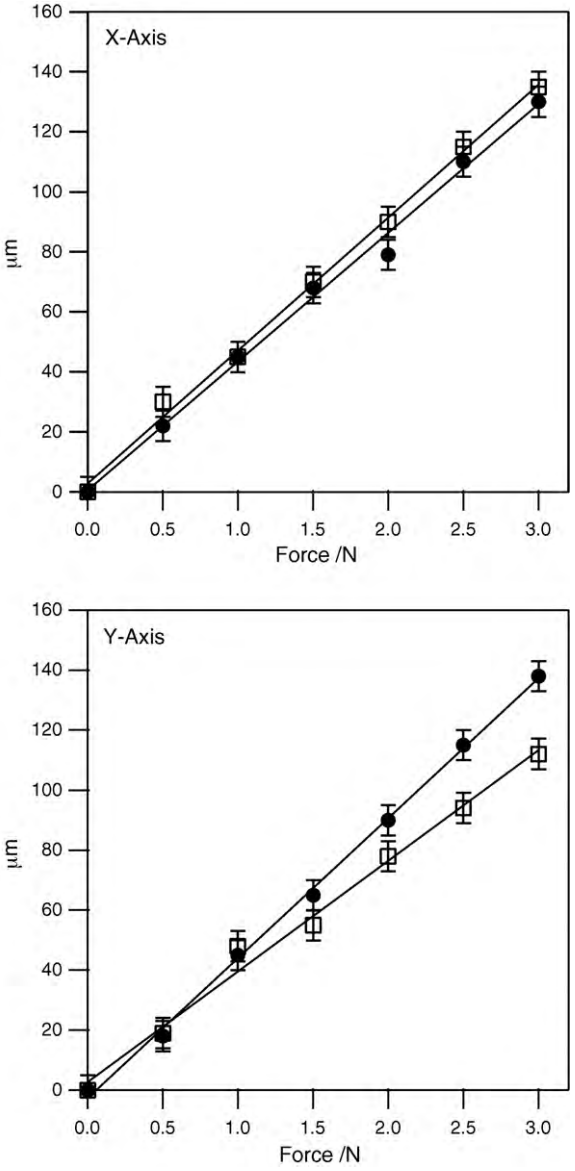

Fig. 3. Displacement curves for the complete flexure guidance mechanism along the x (top) and y (bottom) directions. The circles (squares) represent the displacement of the flexure by pulling along the forward (reverse) direction. The error bars are given by the accuracy of the micrometer gauge.

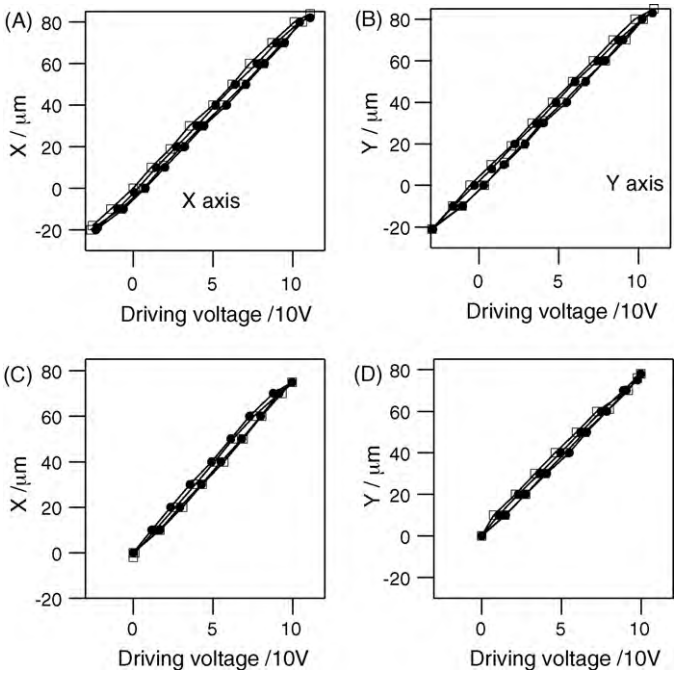

Fig. 4. Displacement of the scanning stage driven by the piezoelectric actuators. Panels A and B were obtained with the actuators driven in open loop and panels C and D correspond to closed-loop. The open squares represent the travel of the free actuators and solid circles represent the travel of the actuators when driving the stage.

Fig. 3 shows the displacement curves in the two directions of motion of the guidance mechanism for the 0–3 N range of forces by using a micrometer dial indicator with a resolution of 5 μm. A fairly linear relationship is found. The differences in the slopes are due to manufacturing tolerances. The experimental values of the static stiffness obtained from a linear fit to the data shown in Fig. 3 are $k_x^+ = 21.0(5)$, $k_x^- = 27(7)$, $k_y^+ = 23.0(5)$ and, $k_y^- = 27.0(5)$ mN/μm. The measured values are lower than the target 39 mN/μm for each direction of motion, mainly due to the lower Young's modulus of the actual aluminum alloy.

After attaching the actuators on the stage, we measured the effective displacement of the entire structure by applying a bias to the actuators. The results are shown in Fig. 4.

Some hysteresis is apparent in these curves. The maximum displacement of the actuators only suffered a reduction when operated in the open-loop mode. The largest strokes were 84 and 85 μm for the free actuators, and 82 and 83 μm for the stage loaded actuators. This represents 2.5% difference of the maximum stroke, and is consistent with the constraint set for the dimensioning of the notch thickness. No reduction in the maximum displacement was measured when the actuators were operated in the closed-loop mode. A maximum displacement of 76 μm is obtained for both directions.

3. Performance

To evaluate the merit of the constructed scanning stage for applications in single molecule spectroscopy it was necessary to implement an optical system and the detection electronics. The

Author's personal copy

details of the optical system can be found elsewhere [12]. An inverted microscope Olympus IX71 was used to host the scanning stage. The scanning stage was kinematically mounted on the microscope frame. The excitation laser is introduced through the back port of the microscope and it is focused by the microscope objective. The fluorescence emitted by a sample mounted on the scanning device is collected by the same microscope objective, and imaged on a confocal pinhole (50 μm in diameter). The light that emerges from this pinhole is focused onto an avalanche photodiode detector. Interference reflector (z532 or z405) and filters (HQ580/60 or HQ460/80) are used to suppress the excitation light from reaching the detector. The voltages fed into the input of the high voltage amplifiers were provided by a general purpose data acquisition card (NI-PCI6733). The signal from the avalanche photodetector was connected to a time correlated single photon counting card (Becker and Hickl SPC630). A program written in LabWindows CVI was used to acquire the fluorescence signal and to drive the voltages for scanning the sample. The samples were prepared by casting a single drop of 5×10^{-10} M solution of glass beads or rhodamine dye on a clean cover glass spinning at ca. 2000 rpm.

Fig. 5 shows images of ca. 50–100 nm fluorescent glass beads excited by a diode laser at 405 nm. Panels A-B are the forward and reverse scanning directions, hereafter called trace and retrace images. The image size in A-B is 20 μm × 20 μm while B-C is a 10 μm × 10 μm area rescanned within the marks in A. The fluorescent beads are clearly resolved in these images. The apparent differences among the sizes of the beads within an image, is the result of the spread in brightness that arises from the size polydispersity of the beads. The mean diameter of the beads is 70 nm obtained from TEM micrographs.

The size of the images is set by our rather coarse calibration obtained by fitting the data in Fig. 4 to a straight line. For applications where higher accuracy is needed an interferometric calibration or capacitive position sensing system could be adopted [13–17]. Nevertheless an internal calibration is always available provided that the features in the images are diffraction limited. For this case the point spread function is the convolution of the Airy functions representing the glass bead and the laser focal spot. In the case of a point sized emitting object the full width at half maximum (FWHM) of the Airy feature reduces to [18] FWHM = $\lambda/(2 \times \mathrm{NA})$. For λ = 405 nm, and NA = 1.22, FWHM = 170 nm. In Fig. 5, the line profile across a single glass bead was fit to a Gaussian function with a FWHM = 198 nm. Since the glass beads are 70 nm in diameter, a FWHM = 184 nm is obtained by convoluting two Gaussian functions with FWHM 170 nm and 70 nm. The agreement is rather good considering the simplicity of our calibration.

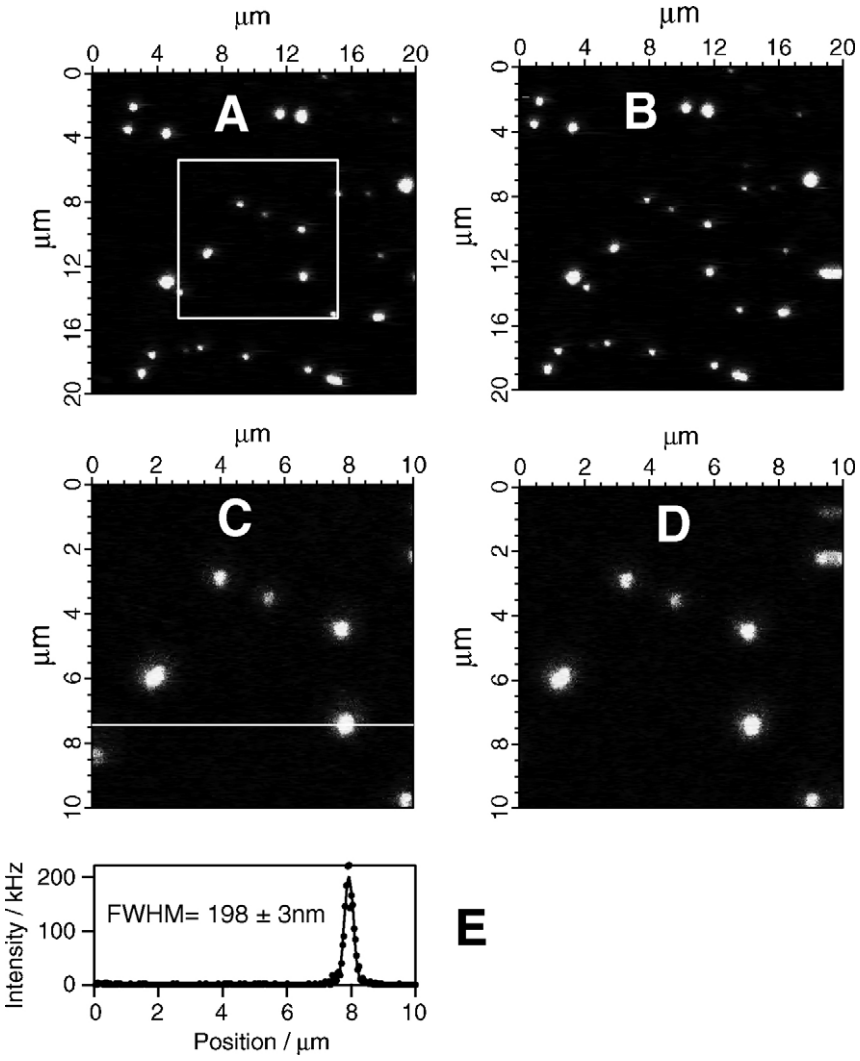

Fig. 5. Images of fluorescent glass beads collected in forward (A and C) and backward (B and D) motion. The size of the scanned area in (A) and (B) is 20 μm × 20 μm. The images (C) and (D) correspond to the 10 μm × 10 μm squared area bound by the four crosses in (A). The data shown in (E) is an intensity profile across a bead and along the line shown in (C). The fit is a Gaussian function.

Author's personal copy

Due to a phase lag when the stage is driven by the electrical signal, there is a difference between the actual and the target positions. The origin of this phase lag is mainly the limited bandwidth of the scanning stage and electronics. This produces a hysteretic behavior in the forward–backward intensity traces across fluorescent objects in the sample. By collecting the image in the forward and reverse directions of motion, it is possible to quantify the hysteresis in real-time. This is necessary to accurately position the focus of the laser beam onto a target molecule for single molecule experiments. Our images contain 256 × 256 pixels and are obtained by counting photons on a given pixel for a preset dwell time before advancing to the next pixel. Since the integration time can vary from a fraction of a ms to a few ms, the scanning speed can vary about one order of magnitude. The smaller the pixel dwell time, the faster would the stage be moving. Because the number of pixels per line scan in our acquisition program is 256 for any image size, larger images imply a larger physical area covered per pixel, which also translates into a higher scanning speed. An assessment of the effect of the scanning speed on the hysteresis was obtained by measuring the offset between the positions of fluorescent beads in the trace and retrace images. We define a relative hysteresis Hrel = image shift/image size. A plot of Hrel versus the reciprocal pixel dwell time is shown in Fig. 6. The shift between the trace and retrace images for different image sizes lay on the same linear relationship with the reciprocal pixel dwell time. This simple dependence can be used to correct the driving voltages applied to the stage when the laser is to be positioned on a target molecule. The scanning stage lags behind the position calculated by the driving voltages. Thus, the trace image or a trace line scan appears shifted away from the origin while the retrace image is shifted towards the origin in the real position axis. It follows that the corrected position is:

$$x_{\text{corr}} = x \mp 0.5 \times \text{Hrel} \times \frac{\text{Scan Range}}{\text{Pixel Time}} \quad (4)$$

The minus sign applies when the stage moves in the forward (trace) direction, and the plus sign when the stage moves in the reverse (retrace) direction. The effects of this shift in the slower y-axis of the image are in general negligible because the line dwell time is N_{Pixels} times larger than the pixel dwell time (in our case $N_{\text{Pixels}} = 256$). By using this correction, the target position of a molecule in a line scan can be corrected and a line-by-line search procedure to detect and target molecules can be implemented. We test this approach by performing simple line scans in a predetermined region of the sample. For each line scan, we execute a simple algorithm that finds the intensity peaks by subsequently fitting a segment of the line scan to a quadratic equation. If the fit exceeds a preset intensity threshold, the pixel position for the maximum of the parabola is recorded. We then apply the aforementioned correction due to the mechanical hysteresis of the scanning stage (Eq. (4)). We repeat the last line scan and stop at the pixel position calculated with the correction. After a 0.5 s delay a shutter is opened, and the fluorescence is collected by keeping the sample steady. Fluorescence versus time traces (fluorescence trajectories) are then obtained for luminescent objects in the sample. The acquisition mode used in our work only needs a threshold to decide if data collection will be initiated on a particular object. There are several advantages of performing the acquisition this way. First, the brighter objects can be studied first, and after all of them have been inspected up to the irreversible photobleaching time the same area can be scanned again, using a lower threshold. Then a second series of objects can be investigated. Second, this scheme suffers from less subjectivity that is commonly associated with manual selection of luminescent objects from an image. Lastly, this scheme can be readily generalized to any number of channels by searching for peaks on the intensity array of a selected channel.

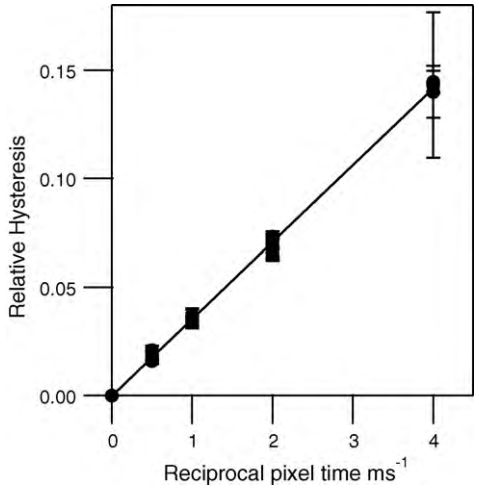

Fig. 6. The hysteretic behavior of the scanning stage obtained from images of fluorescent glass beads.

In this type of experiments, the concern is the ability of the scanning stage to sustain the position over a period of time which is of the order of tens of seconds. Because the point spread function of the system is a sharp function of position, any instability in the position during acquisition of single molecule trajectories will be evident as intensity fluctuations. The major source of these mechanical instabilities are thermal effects [19] and creep [20]. As a zero order picture, we can take the excitation intensity distribution to be a Gaussian function in the x–y directions with a full width at half a maximum of 200 nm. Therefore, a deviation of 100 nm in the molecule position should cause a fluorescence intensity drop of ca. 50%. Such variation of the fluorescence intensity as the target molecule moves slightly to the sides of the diffraction limited laser spot could be readily detected. To conduct this performance tests, we choose the fluorescent dye rhodamine 6G. This dye has nearly 100% fluorescence quantum yield and it is relatively stable against photobleaching. Also, it shows little blinking dynamics. For excitation of this dye at 532 nm we used a 5 mW Nd-vanadate laser. Fluorescence trajectories for single rhodamine 6G are shown in Fig. 7. The data for the upper five traces has been binned in 10 ms bins. A characteristic of a single molecule fluorescence trajectory is the irreversible photobleaching event that abruptly ends the emission of the molecule in a single step. The emission before photobleaching shows a constant intensity. In some cases, fluctuations between two possible intensity states are seen in the trajectory. This is the well-known blinking dynamics. Single molecule trajectories terminate abruptly by irreversible photobleaching which brings the intensity back to the background signal. Another control experiment was done in which the fluorescence signal from a droplet of solution of rhodamine 6G in water (100 nM) was collected over a period of over 1 min. In this experiment, an average number on the order of 10^3 molecules is present in the observation volume. Because the molecules are free to diffuse in and out of the illuminated region, photobleaching will not significantly affect the fluorescence intensity.

Since the solution is homogeneous, variations of the position of the focal spot, and thus the mechanical stability of the scanning stage, have no effect on the fluorescence intensity trajectory. Under these conditions, the only source of intensity fluctuations is the laser intensity noise. The bottom panel in Fig. 7 shows the fluorescence signal obtained from a solution of rhodamine 6G. The time axis has been binned into 20 ms bins. A comparison between the fluorescence trajectories for single molecules and the solution

Author's personal copy

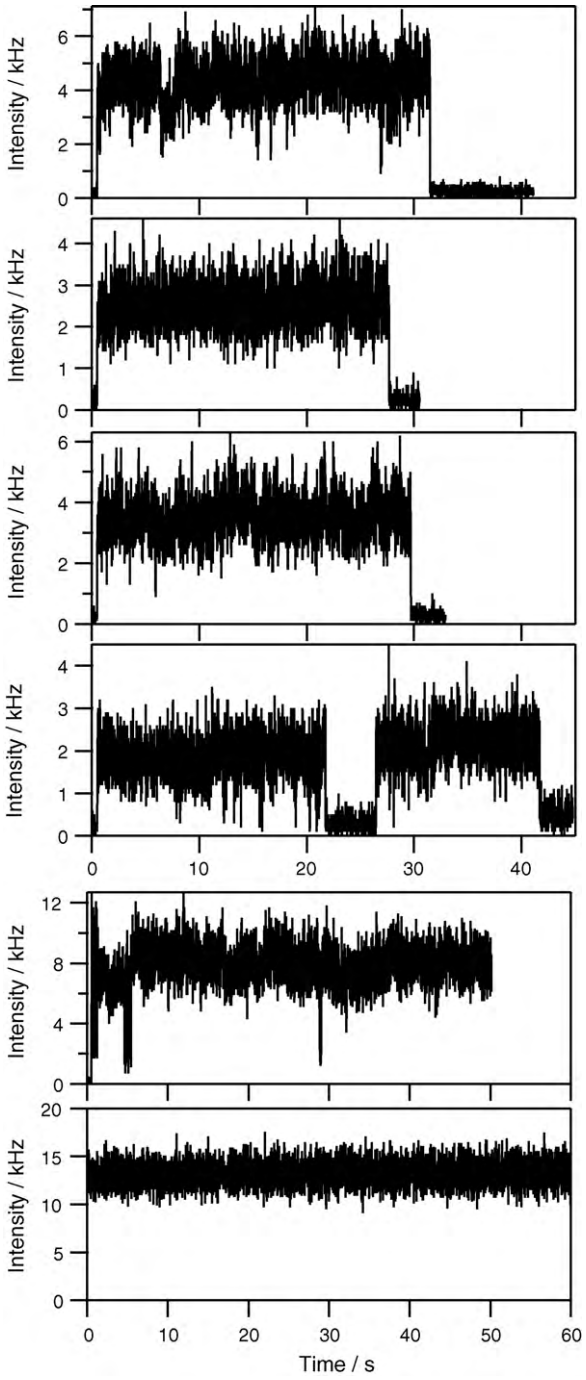

Fig. 7. Fluorescence trajectories for rhodamine 6G molecules.

experiment reveals very similar intensity stabilities. The fluorescence trajectories obtained with the scanning stage described in this article show very stable intensity values over the lifespan of the single molecules. This position stability is essential for the application pursued for this setup. Although we are not interested in the operation of this scanning stage without using the built in feedback of the piezoelectric actuators, we conducted tests in open-loop mode. Images obtained with the actuators operated in open loop mode had acceptable quality with ca. 100 nm drift of the image center from one image to the next. Trajectories collected by the procedure described above but without the use of the feedback loop on the actuators lead to decaying intensities reaching background within ca. 30 s.

To further demonstrate the performance of the present setup, we carried out experiments in which a polarizer is inserted into the optical path of the fluorescence, which is the split in to S and P with respect to the polarizer. For each of the two polarizations the fluorescence then traverses an interference filter, and it is then detected by a single photon counting avalanche photodiode module. Excitation of the fluorescence with linearly polarized light at 532 nm was then carried out for the rhodamine 101 molecules deposited on a clean glass surface. Rhodamine 101 was chosen for this experiment because its transmission through the pair of interference filters used in our setup, and high quantum yield of fluorescence. A common practice in single molecule imaging, is to combine the images of multiple channels in a color coded image. This was done for our polarization resolved channels. The images obtained by the two detectors are rendered with green only RGB values for S polarization, and with red only RGB values for the P polarization. Upon addition of the images of the two channels, a red-green rendering is obtained that clearly shows any polarization changes in the fluorescence during the collection of the fluorescence image. These changes arise from fluctuations in the orientation of the molecule, which modifies the direction of the molecular transition dipole moment. The polarization of the emission tracks the changes in the molecular orientation. Fig. 8 shows a fluorescence image of individual rhodamine 101 molecules on a glass surface. The image is ca. 4 μm × 4 μm in size. Thermal fluctuations in the molecule orientation are seen in the images as red lines of pixels on the green spot in Fig. 8. The yellow spot arises from a molecule whose orientation yields nearly equal signals in the S and P detectors. Fluorescence trajectories for single rhodamine 101 molecules are shown in Fig. 9. The trajectories further confirm the orientational jumps experienced by rhodamine 101 molecules. In the top two trajectories, clearly anticorrelated fluctuation in the S and P polarizations are seen, which is consistent with nearly 90° rotation of the transition dipole moment in the plane of the plane perpendicular to the optical axis. Motion of the transition dipole moment towards the optical axis, will cause correlated fluctuations in the intensities observed in the S and P detectors. This is seen on the bottom two trajectories of Fig. 9.

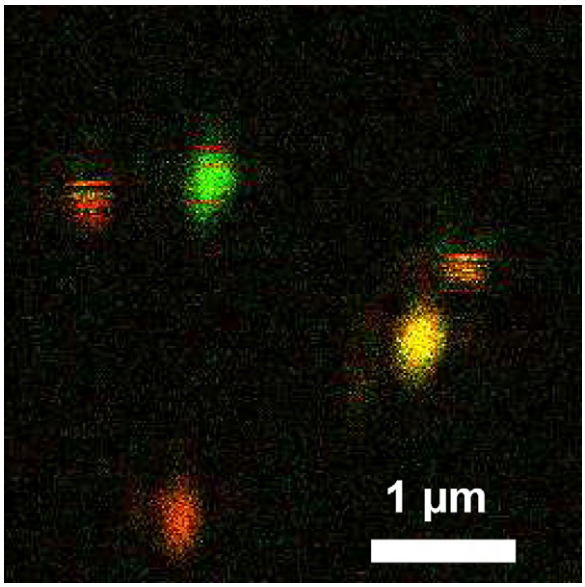

Fig. 8. Fluorescence image for rhodamine 101 molecules obtained with polarization resolved detection. The green (red) line represent the S(P) polarized emission. The intensity ranges from 0 to 8.0 kHz. The excitation was 360 nW measured on the front of the microscope objective. (For interpretation of the references to color in this figure legend, the reader is referred to the web version of the article.)

Author's personal copy

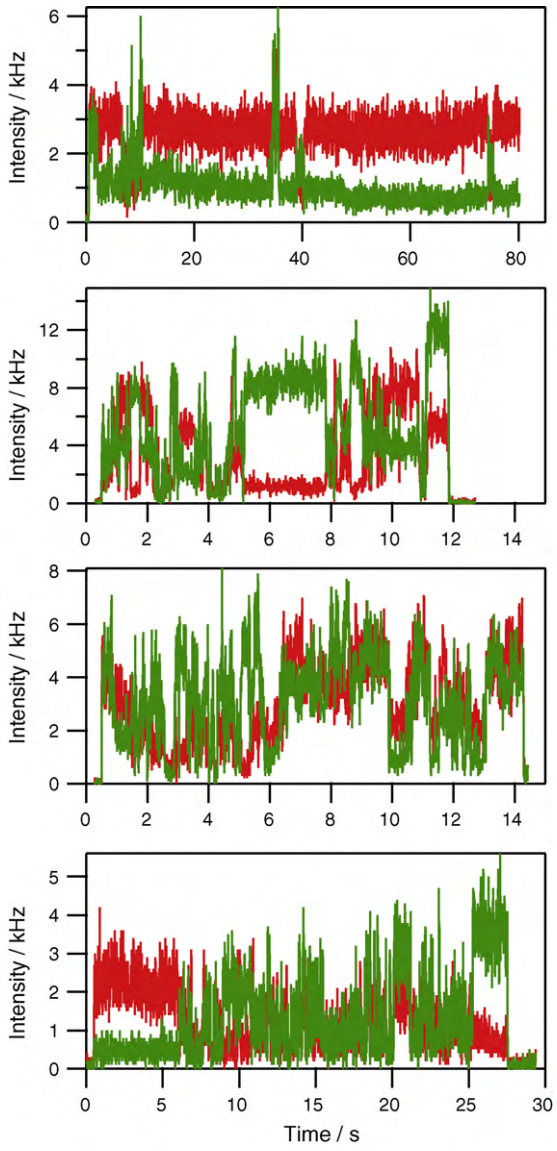

Fig. 9. Fluorescence trajectories for rhodamine 101 molecules obtained with polarization resolved detection. The green (red) line represents the S(P) polarized emission. (For interpretation of the references to color in this figure legend, the reader is referred to the web version of the article.)

4. Conclusions

A simple sample scanning device suitable for single molecule spectroscopy applications was developed. Sub-micrometer resolution images were demonstrated. The correction to the mechanical imperfections of this scanning mechanism is obtained by measuring the shift between forward and reverse motion collected images. Positioning the laser beam over a single molecule for collection of fluorescence trajectories can be done within the diffraction limited spot size by applying the correction to the hysteresis of the scanning mechanism. The main contribution of this paper is a simple method for accurately positioning the laser onto single molecules when the scanning stage is driven relatively fast relative to the feedback mechanism. The performance of this scanning device was demonstrated by representative single molecule fluorescence images and trajectories.

The scanning device may be used in applications other than single molecule spectroscopy, such as fluorescence readout machines for microarray sensors.

Acknowledgements

We thank Dr. Mariano Bossi at Department of NanoBiophotonik (200) Max Plank Institute for Biophysical Chemistry, for his kind gift of the fluorescent glass beads and Prof. Pedro Aramendia from The Department of Chemistry, University of Buenos Aires for giving us the rhodamine dye samples. A. Rasamessard was supported by the Thailand Research Fund through the Royal Golden Jubilee scholarship. We thank NSTDA for a TGIST scholarship supporting Ph.D. student Ketvalee Treegate. A-TEAM is kindly acknowledged for the precision wire-cut fabrication service.

Appendix A. Supplementary data

Supplementary data associated with this article can be found, in the online version, at doi:10.1016/j.snb.2010.07.008.

References

[1] W.E. Moerner, A dozen years of single-molecule spectroscopy in physics and chemistry and biophysics, J. Phys. Chem. B 106 (2002) 910–927.
[2] A. Squire, P.I.H. Bastiaens, Three dimensional image restoration in fluorescence lifetime imaging microscopy, J. Microsc. (Oxford) 193 (1999) 36–49.
[3] X.S. Xie, J.K. Trautman, Optical studies of single molecules at room temperature, Annu. Rev. Phys. Chem. 49 (1998) 441–480.
[4] S. Awtar, A.H. Slocum, Constraint-based design of parallel kinematic XY flexure mechanisms, ASME J. Mech. Design 119 (2007) 816–830.
[5] S. Awtar, A.H. Slocum, E. Sevincer, Characteristics of beam-based flexure modules, ASME J. Mech. Design 119 (2007) 225–639.
[6] C.L. Chu, S.H. Fan, A novel long-travel piezoelectric-driven linear nanopositioning stage, Precis. Eng. J. Int. Soc. Precis. Eng. Nanotechnol. 30 (2006) 85–95.
[7] S.B. Choi, S.S. Han, Y.S. Lee, Fine motion control of a moving stage using a piezoactuator associated with a displacement amplifier, Smart Mater. Struct. 14 (2005) 222–230.
[8] K.-B. Choi, D.-H. Kim, Monolithic parallel linear compliant mechanism for two axes ultraprecision linear motion, Rev. Sci. Instrum. 77 (2006) 065106.
[9] A.G. Smith, C.B. David, Handbook of Single Molecule Fluorescence Spectroscopy, Oxford University Press, Oxford, 2006, p. 280.
[10] S.T. Smith, Flexures: Elements of Elastic Mechanisms, Gordon and Breach Science Publishers, Elsevier, 2000, p. 448.
[11] S. Devasia, E. Eleftheriou, S.O.R. Moheimani, A survey of control issues in nanopositioning, IEEE Trans. Contr. Sys. Technol. 15 (2007) 802–823.
[12] J.H. Hodak, C.D. Downey, J.L. Fiore, A. Pardi, D.J. Nesbitt, Docking kinetics and equilibrium of a GAAA tetraloop–receptor motif probed by single-molecule FRET, Proc. Natl. Acad. Sci. 102 (2005) 10505–10510.
[13] H.G. Xu, T. Ono, M. Esashi, Precise motion control of a nanopositioning PZT microstage using integrated capacitive displacement sensors, J. Micromech. Microeng. 16 (2006) 2747–2754.
[14] H.C. Yeh, W.T. Ni, S.S. Pan, Real-time motion control with subnanometer heterodyne interferometry, Int. J. Modern Phys. D 11 (2002) 1087–1099.
[15] H.C. Yeh, W.T. Ni, S.S. Pan, Digital closed-loop nanopositioning using rectilinear flexure stage and laser interferometry, Control Eng. Pract. 13 (2005) 559–566.
[16] G. Schitter, A. Stemmer, Fast closed loop control of piezoelectric transducers, J. Vac. Sci. Technol. B 20 (2002) 350–352.
[17] G. Schitter, R.W. Stark, A. Stemmer, Sensors for closed-loop piezo control: strain gauges versus optical sensors, Meas. Sci. Technol. 13 (2002) N47–N48.
[18] S.W. Hell, Far-field optical nanoscopy, Science 316 (2007) 1153–1156.
[19] J. Pritchard, R. Ramesh, C.R. Bowen, Time–temperature profiles of multi-layer actuators, Sens. Actuators A: Phys. 115 (2004) 140–145.
[20] H. Jung, D.-G. Gweon, Creep characteristics of piezoelectric actuators, Rev. Sci. Instrum. 71 (2000) 1896–1900.

Biographies

Ketvalee Treegate was born in Lopburi, Thailand, on August 25, 1984. She is receiving her Ph.D. degree in physics from The Faculty of Science, Mahidol University, Bangkok, Thailand, in 2010. Ketvalee Treegate has been working as a research assistant in the Department of Physics of Mahidol University and has been awarded a TGIST scholarship from the National Science Development Agency of Thailand. Her research is on single molecule spectroscopy and studies of iron and iron boride magnetic nanoparticles.

Areefen Rasamessard was born in Yala, Thailand on July 24, 1980. He received his Ph.D. degree in physics from The Faculty of Science, Mahidol University, Bangkok, Thailand, in October, 2009. He has been working as a research assistant in the Department of Physics of Mahidol University, and also at Academia Sinica at Taiwan where he carried out fluorescence experiments on single aggregates of luminescent polymers. His research interests are in the fields of light emitting polymers.

Author's personal copy

Tanakorn Osotchan was born in Pathumthani, Thailand on November 22, 1965. He obtained a Ph.D. degree in semiconductor physics from Macquarie University, New South Wales, Australia in 1995. Now, he is assistant professor at the Department of Physics, Mahidol University, Bangkok, Thailand. His research interests are organic based light emitting displays and semiconductor physics.

Jose Hector Hodak was born in 1968 in Buenos Aires, Argentina. He obtained his Ph.D. in Physical Chemistry at University of Notre Dame, Indiana, USA, in 2001 studying the ultra-fast dynamics of metal nanoparticles. Dr. Hodak worked from 2001 to 2004 as a postdoctoral researcher at JILA-University of Colorado, where he carried out single molecule fluorescence experiments in RNA. He worked as researcher at the Department of Physics, Mahidol University from 2005 until 2010. He is currently an independent investigator of CONICET and assistant professor at the University of Buenos Aires. His research interests are single molecule and ultrafast spectroscopies.